Gravitational Form Factors of the Proton from Lattice QCD

Daniel C. Hackett,[1,2] Dimitra A. Pefkou,[3,2,4] and Phiala E. Shanahan[2]
[1]Fermi National Accelerator Laboratory, Batavia, Illinois 60510, USA
[2]Center for Theoretical Physics, Massachusetts Institute of Technology, Cambridge, Massachusetts 02139, USA
[3]Department of Physics, University of California, Berkeley, California 94720, USA
[4]Nuclear Science Division, Lawrence Berkeley National Laboratory, Berkeley, California 94720, USA

(Received 24 October 2023; accepted 22 May 2024; published 21 June 2024)

The gravitational form factors (GFFs) of a hadron encode fundamental aspects of its structure, including its shape and size as defined from, e.g., its energy density. This Letter presents a determination of the flavor decomposition of the GFFs of the proton from lattice QCD, in the kinematic region $0 \leq -t \leq 2$ GeV^2. The decomposition into up-, down-, strange-quark, and gluon contributions provides first-principles constraints on the role of each constituent in generating key proton structure observables, such as its mechanical radius, mass radius, and D term.

DOI: 10.1103/PhysRevLett.132.251904

Achieving a quantitative description of the structure of the proton and other hadrons in terms of their quark and gluon constituents is a defining challenge for hadronic physics research. The gravitational structure of the proton, encoded in its gravitational form factors (GFFs), has come under particular investigation [1–23] since the first extraction of one of its GFFs from experimental measurements in 2018 [24]. Defined from the matrix elements of the energy-momentum tensor (EMT) in a hadron state, GFFs describe fundamental properties such as the mass and spin of a state, the less well-known but equally fundamental D term (or "Druck" term), and information that can be interpreted in terms of the distributions of energy, angular momentum, and various mechanical properties of the system [25–28].

The proton GFFs $A(t)$, $J(t)$, and $D(t)$ are defined as

$$\begin{aligned}\langle N(\mathbf{p}',s')|\hat{T}^{\mu\nu}|N(\mathbf{p},s)\rangle &= \frac{1}{m}\bar{u}(\mathbf{p}',s')\Big[P^\mu P^\nu A(t) + iP^{\{\mu}\sigma^{\nu\}\rho}\Delta_\rho J(t) \\ &\quad + \frac{1}{4}(\Delta^\mu\Delta^\nu - g^{\mu\nu}\Delta^2)D(t)\Big]u(\mathbf{p},s), \end{aligned} \tag{1}$$

where $a^{\{\mu}b^{\nu\}} = (a^\mu b^\nu + a^\nu b^\mu)/2$, $N(\mathbf{p},s)$ is a proton state with three-momentum $\mathbf{p}$ and spin eigenvalue $s = \pm\frac{1}{2}$, $u(\mathbf{p},s)$ is the Dirac spinor, $P = (p+p')/2$, $\Delta = p' - p$, $t = \Delta^2$, and $\sigma_{\mu\nu} = \frac{i}{2}[\gamma_\mu,\gamma_\nu]$, where γ_μ are the Dirac matrices. $\hat{T}^{\mu\nu}$ is the renormalization-scale-independent [29] symmetric EMT of QCD [30]. It can be decomposed into quark and gluon contributions as $\hat{T}^{\mu\nu} = \sum_{i\in\{q,g\}}\hat{T}^{\mu\nu}_i$, where

$$\begin{aligned}\hat{T}^{\mu\nu}_g &= 2\mathrm{Tr}\left[-F^{\mu\alpha}F^\nu_\alpha + \frac{1}{4}g^{\mu\nu}F^{\alpha\beta}F_{\alpha\beta}\right], \\ \hat{T}^{\mu\nu}_q &= \sum_f [i\bar{\psi}_f D^{\{\mu}\gamma^{\nu\}}\psi_f], \end{aligned} \tag{2}$$

$F^{\mu\alpha}$ is the gluon field strength tensor, ψ_f is a quark field of flavor f, and $D^\mu = \partial^\mu + igA^\mu$ is the covariant derivative. The matrix elements of $\hat{T}^{\mu\nu}_i$ define the renormalization scheme- and scale-dependent partonic contributions to the GFFs, which can also be interpreted as moments of generalized parton distributions (GPDs) [31–33]. The corresponding forward limits $A_i(0)$, $J_i(0)$, and $D_i(0)$ describe the partonic decomposition of the proton's momentum, spin, and D term, respectively. Poincaré symmetry imposes the sum rules [8,32,34–36] $A(0) = 1$ and $J(0) = 1/2$, while the value of $D(0)$ is conserved but not constrained from spacetime symmetries [37]. The t dependence of the GFFs encodes additional information about the quark and gluon contributions to densities in the proton [25–27]. While determination of the flavor decomposition of the proton's momentum and spin has a long history, reviewed in Refs. [38–41], constraints on the D term [17–20,24,42,43] and the t dependence [17–21,43–45] of the proton's GFFs have been comparatively recent.

This Letter presents a flavor decomposition of the total GFFs of the proton, $A(t)$, $J(t)$, and $D(t)$, into gluon, up-, down-, and strange-quark contributions, achieved through a lattice QCD calculation with quark masses yielding a close-to-physical value of the pion mass. The $D_{u+d}(t)$ and $D_g(t)$ GFFs are found to be consistent with the recent

experimental extractions of these quantities [24,42], while the t dependence of $A_g(t)$ is consistent with one of the two analyses of experimental data presented in Ref. [42] and in tension with the other (including the updated analysis of Ref. [46]). The individual up-, down-, and strange-quark GFFs are quantified for the first time from experiment or first-principles theory, albeit on a single lattice QCD ensemble, but fully accounting for mixing with the gluon contribution. From the GFFs, the energy and radial force densities of the proton, and the associated mass and mechanical radii, are computed, allowing a quantitative comparison of these different measures of the proton's size.

Lattice QCD calculation.—The lattice QCD calculation is performed using a single ensemble of gauge field configurations generated by the JLab/LANL/MIT/WM groups [47], using the Lüscher-Weisz gauge action [48] and $N_f = 2 + 1$ flavors of clover-improved Wilson quarks [49] with clover coefficient set to the tree-level tadpole-improved value and constructed using stout-smeared links [50]. The light-quark masses are tuned to yield a pion mass of $m_\pi \approx 170$ MeV, and the lattice spacing and volume are $a \approx 0.091$ fm [51,52] and $L^3 \times T = 48^3 \times 96$, respectively. The technical details of the lattice QCD calculation are as for the determination of the pion GFFs in Ref. [53] and are summarized below. Additional details, including analysis hyperparameter choices and figures illustrating intermediate results, are included in Supplemental Material [54].

First, the bare matrix elements of $\hat{T}^{\mu\nu}_g$, and of the singlet and nonsinglet quark flavor combinations of the EMT, i.e.,

$$\text{singlet:}\ \hat{T}^{\mu\nu}_q = \hat{T}^{\mu\nu}_u + \hat{T}^{\mu\nu}_d + \hat{T}^{\mu\nu}_s, \tag{3}$$

$$\text{nonsinglet:}\ \hat{T}^{\mu\nu}_{v_1} = \hat{T}^{\mu\nu}_u - \hat{T}^{\mu\nu}_d, \tag{4}$$

$$\hat{T}^{\mu\nu}_{v_2} = \hat{T}^{\mu\nu}_u + \hat{T}^{\mu\nu}_d - 2\hat{T}^{\mu\nu}_s, \tag{5}$$

are constrained from ratios of three-point and two-point functions that are proportional to the bare matrix elements of the EMT [Eq. (1)] at large Euclidean times. The three-point function of the gluon EMT is measured on 2511 configurations, averaged over 1024 source positions per configuration, with the gluon EMT measured on gauge fields that have been Wilson flowed [55–57] to $t_{\text{flow}}/a^2 = 2$, for all sink and operator momenta with $|\mathbf{p}'|^2 \le 10(2\pi/L)^2$ and $|\mathbf{\Delta}|^2 \le 25(2\pi/L)^2$ and all four spin channels $s, s' \in \{\pm 1/2\}$. The connected part of the quark three-point function is measured on 1381 configurations using the sequential source method, inverting through the sink for 11 choices of source-sink separation in the range $[6a, 18a]$, with the number of sources varying between 9 and 32 for the different source-sink separations. The momenta measured are $\mathbf{p}' \in 2\pi/L\{(1,0,-1),(-2,-1,0),(-1,-1,-1)\}$ and all $\mathbf{\Delta}$ with $|\mathbf{\Delta}|^2 \le 25(2\pi/L)^2$, for a single spin channel with $s = s' = 1/2$. The disconnected parts are stochastically estimated on the same 1381 configurations as the connected parts, using two samples of Z_4 noise [58], diluting in spacetime using hierarchical probing [59,60] with 512 Hadamard vectors, and computing the spin-color trace exactly. Measurements are made for all $|\mathbf{p}'|^2 \le 10(2\pi/L)^2$, $|\mathbf{\Delta}|^2 \le 25(2\pi/L)^2$, and all four spin channels.

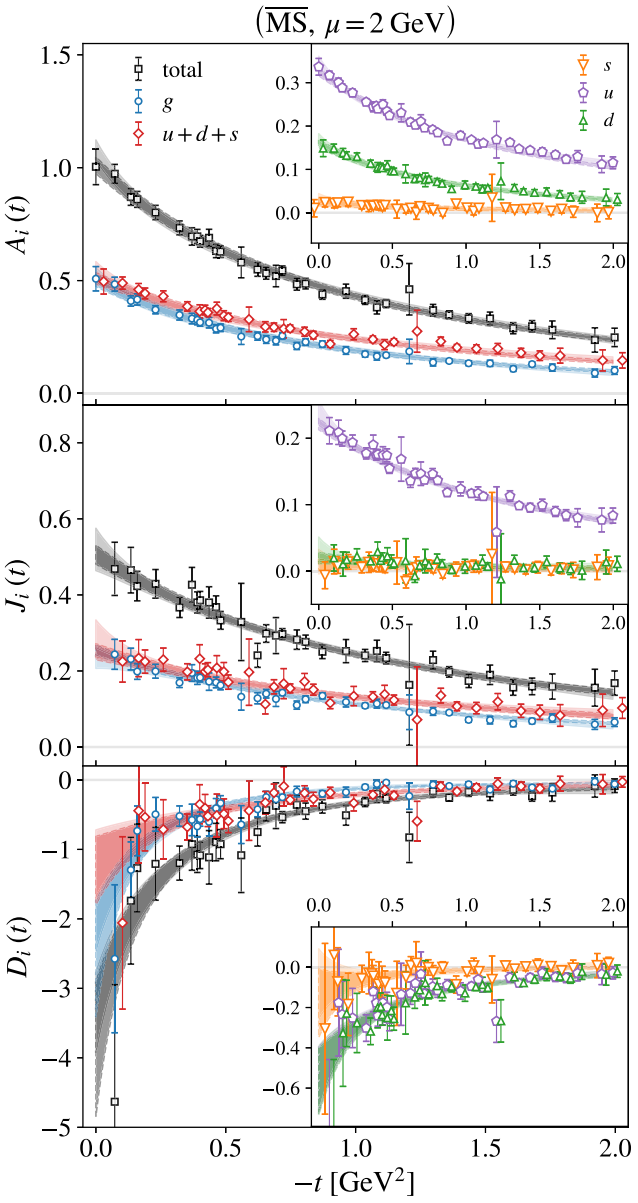

FIG. 1. The three GFFs of the proton, computed on the lattice QCD ensemble of this Letter, and their decomposition into gluon and total quark contributions, are shown as functions of t. Inset figures show the isosinglet quark GFFs further decomposed into up-, down-, and strange-quark contributions. The total GFFs are renormalization scheme and scale independent, while all other GFFs are shown in the $\overline{\text{MS}}$ scheme at $\mu = 2$ GeV. The dark bands represent dipole fits to the data in the case of g and $q = u + d + s$ and linear combinations of the dipole fits to q, v_1, and v_2 in all other cases. The lighter bands show analogous fits using the z expansion.

Second, ratios of three- and two-point functions that correspond to the same linear combination of GFFs—as

TABLE I. The flavor decomposition of the momentum fraction, spin, and D term of the proton, computed on the lattice QCD ensemble of this Letter, obtained from dipole and z-expansion fits to the proton GFFs, renormalized at $\mu = 2$ GeV in the $\overline{\text{MS}}$ scheme. The fit parameters of the two models are included in Supplemental Material [54].

	Dipole			z expansion		
	$A_i(0)$	$J_i(0)$	$D_i(0)$	$A_i(0)$	$J_i(0)$	$D_i(0)$
u	0.3255(92)	0.2213(85)	−0.56(17)	0.349(11)	0.238(18)	−0.56(17)
d	0.1590(92)	0.0197(85)	−0.57(17)	0.171(11)	0.033(18)	−0.56(17)
s	0.0257(95)	0.0097(82)	−0.18(17)	0.032(12)	0.014(19)	−0.08(17)
$u+d+s$	0.510(25)	0.251(21)	−1.30(49)	0.552(31)	0.286(48)	−1.20(48)
g	0.501(27)	0.255(13)	−2.57(84)	0.526(31)	0.234(27)	−2.15(32)
Total	1.011(37)	0.506(25)	−3.87(97)	1.079(44)	0.520(55)	−3.35(58)

defined in Eq. (1) and up to an overall sign—are averaged. The summation method [61–64] is used to fit the Euclidean time dependence of the averaged ratios and extract the bare matrix elements. In all cases, 1000 bootstrap ensembles are used to estimate statistical uncertainties, and systematic uncertainties in fits are propagated using model averaging with weights dictated by the Akaike information criterion [65–68]. Since connected measurements exist for only a subset of the matrix elements, the disconnected contributions to the bare GFFs of T_q and T_{v_2} (T_{v_1} is purely connected, as the disconnected contributions cancel in the difference) are fit separately using all available data, with the results used to obtain better constraints for the subset for which connected parts are available and, thus, to obtain the full matrix elements of T_q and T_{v_2}. Finally, the matrix elements are divided into $34t$ bins using k-means clustering [69], and the GFFs are extracted by solving the resulting linear systems of equations, with the renormalization performed nonperturbatively using the results and procedure presented in Ref. [53].

Results.—The flavor decomposition of the renormalized GFFs, computed on the lattice QCD ensemble of this Letter, is presented in Fig. 1. To guide the eye, the GFFs of currents g and q are fit using both a multipole ansatz with $n = 2$ (dipole), chosen as the integer yielding the lowest χ^2 per degree of freedom for the majority of the fits, as well as the more expressive z expansion [70]. The GFFs are further decomposed to yield the individual quark flavor contributions $\mathbf{G}(t) = [A(t), J(t), D(t)]$ from the data and fits for currents q, v_1, and v_2, using

$$\mathbf{G}_u(t) = \frac{1}{3}\mathbf{G}_q(t) + \frac{1}{6}\mathbf{G}_{v_2}(t) + \frac{1}{2}\mathbf{G}_{v_1}(t), \tag{6}$$

$$\mathbf{G}_d(t) = \frac{1}{3}\mathbf{G}_q(t) + \frac{1}{6}\mathbf{G}_{v_2}(t) - \frac{1}{2}\mathbf{G}_{v_1}(t), \tag{7}$$

$$\mathbf{G}_s(t) = \frac{1}{3}\mathbf{G}_q(t) - \frac{1}{3}\mathbf{G}_{v_2}(t). \tag{8}$$

The functional forms of the fit models, along with the resulting fit parameters, are given in Supplemental Material [54].

The flavor decomposition of the forward limits $A(0)$, $J(0)$, and $D(0)$ is summarized in Table I and can be compared with other recent lattice QCD calculations of the decomposition of the momentum and spin fractions of the proton. Specifically, recent studies of the forward-limit quantities at or extrapolated to the physical pion mass report $A_q(0) = 0.491(20)(23)$, $A_g(0) = 0.509(20)(23)$, $J_q(0) = 0.270(11)(22)$, and $J_g(0) = 0.231(11)(22)$ [71], $A_q(0) = 0.618(60)$, $A_g(0) = 0.427(92)$, $J_q(0) = 0.285(45)$, and $J_g(0) = 0.187(46)$ [72], and $A_g(0) = 0.492(52)(49)$ [38]. In the present calculation, the sum rules for the total momentum fraction and spin are satisfied, and the total quark and gluon contributions to these quantities are approximately equal. The calculated gluon momentum fraction is, however, several standard deviations larger than the global fit result $A_g(0) = 0.414(8)$ [73], which can likely be attributed to remaining systematic uncertainties that could not be estimated from this calculation using a single ensemble of lattice QCD gauge fields. In particular, the continuum limit has not been taken, and renormalization coefficients were computed on an ensemble with larger lattice spacing and quark masses [53]. Moreover, the $m_\pi L \approx 3.8$ of the ensemble used in this Letter is less than the typical rule-of-thumb bound $m_\pi L > 4$ targeted to limit finite volume effects to the percent level. The expected magnitudes of these various additional sources of systematic uncertainty are discussed in Supplemental Material [54]. The calculated result for the total D term satisfies the chiral perturbation theory prediction for its upper bound [74], $D(0)/m \leq -1.1(1)$ GeV^{-1}, and is in agreement with chiral models [75–81].

Figure 2 presents a comparison of the dipole fit results with the available experimentally constrained multipole parametrization results for D_{u+d}, A_g, and D_g, presented in Refs. [24,42,46]. The fits to D_{u+d} are found to be consistent, but the uncertainties of the lattice data are comparatively large at the small values of $|t|$ for which experimental data are available. Extractions from new [82] and future experimental data over a larger $|t|$ range, as well as better control of the uncertainties of the lattice QCD result at low $|t|$, will be necessary for a robust comparison.

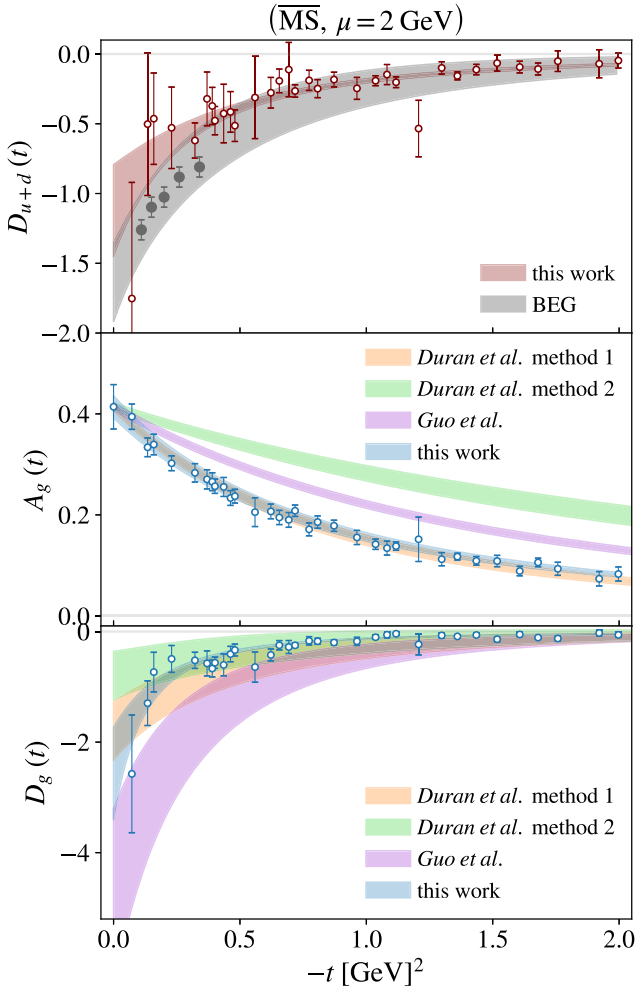

FIG. 2. The proton GFFs $A_g(t)$, $D_g(t)$, and $D_{u+d}(t)$ and corresponding dipole fits, computed on the lattice QCD ensemble of this Letter, are compared with the experimentally constrained multipole parametrizations of Refs. [24] (BEG), [42] (Duran *et al.*), and [46] (Guo *et al.*). For this comparison, the results for $A_g(t)$ are rescaled such that the gluon momentum fraction is $A_g(0) = 0.414(8)$ [73], which is the value used as an input in the extraction in Refs. [42,46]. This does not affect the t dependence of the GFF.

For the gluon GFFs, the lattice QCD results are found to be consistent with the "holographic QCD" inspired approach [14,15] (method 1) to the analysis of experimental data in Ref. [42] and disfavor the "generalized parton distribution" (GPD) inspired approach [83] (method 2). A more recent analysis [46] including an update to the GPD-inspired analysis method, as well as additional experimental data [84], is in less tension with the lattice QCD results presented here. These comparisons illustrate the continued synergy and complementarity between lattice and experimental results for these quantities.

Densities.—Through the definition in terms of the EMT, and by analogy to mechanical systems, the t dependence of the GFFs also gives insight into various densities in the proton. (The physical significance of these analogies is debated [85–88].) Specifically, the Breit-frame distributions $\varepsilon_i(r)$, $p_i(r)$, and $s_i(r)$, defined as

$$\varepsilon_i(r) = m\left[A_i(t) - \frac{t[D_i(t) + A_i(t) - 2J_i(t)]}{4m^2}\right]_{\text{FT}}, \quad (9)$$

$$p_i(r) = \frac{1}{6m}\frac{1}{r^2}\frac{d}{dr}r^2\frac{d}{dr}[D_i(t)]_{\text{FT}}, \quad (10)$$

$$s_i(r) = -\frac{1}{4m}r\frac{d}{dr}\frac{1}{r}\frac{d}{dr}[D_i(t)]_{\text{FT}}, \quad (11)$$

where $r = |\mathbf{r}|$,

$$[f(t)]_{\text{FT}} = \int \frac{d^3\mathbf{\Delta}}{(2\pi)^3}e^{-i\mathbf{\Delta}\cdot\mathbf{r}}f(t), \quad (12)$$

and $i \in \{q, g, q+g\}$, can be interpreted as energy, pressure, and shear force distributions, respectively [25–27]. [The quark and gluon contributions to the pressure and energy densities additionally depend on the GFF $\bar{c}_i(t)$, which appears in the decomposition of the matrix elements of $\hat{T}_i^{\mu\nu}$ due to the quark and gluon EMT terms not being individually conserved. This contribution, which is not constrained in this Letter, vanishes for the total densities, since $\bar{c}_q(t) + \bar{c}_g(t) = 0$.] The root-mean-square radii of the energy density and the longitudinal force density

$$F_i^{||}(r) = p_i(r) + 2s_i(r)/3 \quad (13)$$

yield the mass and mechanical radii of the proton [27]:

$$\langle r_i^2\rangle^{\text{mass}} = \frac{\int d^3\mathbf{r}r^2\varepsilon_i(r)}{\int d^3\mathbf{r}\varepsilon_i(r)},$$
$$\langle r_i^2\rangle^{\text{mech}} = \frac{\int d^3\mathbf{r}r^2F_i^{||}(r)}{\int d^3\mathbf{r}F_i^{||}(r)}. \quad (14)$$

Figure 3 shows the quark, gluon, and total densities and corresponding radii obtained analytically from the dipole fits to the GFFs. For both densities, the gluonic radius is found to be larger than the quark radius. For the case of the gluon mass radius, the result is consistent with that predicted using the holographic QCD-inspired model in the phenomenological extraction of Ref. [42] and the updated analysis of Ref. [46], as shown in Fig. 4. The results for the quark mechanical radius are consistent with a recent extraction from deeply virtual Compton scattering cross section data [89]. They are also consistent with the soliton model prediction [75,80] that the proton mechanical radius is slightly smaller than the charge radius [90] and with the equality of the two radii in the nonrelativistic limit shown in the bag model [1,8].

Summary.—The flavor decomposition of the proton's $A(t)$, $J(t)$, and $D(t)$ GFFs into their up-, down-, strange-quark, and gluon contributions is determined for the first time for a kinematic range $0 \le -t \le 2\ \text{GeV}^2$, using a first-principles lattice QCD calculation. The results reveal that,

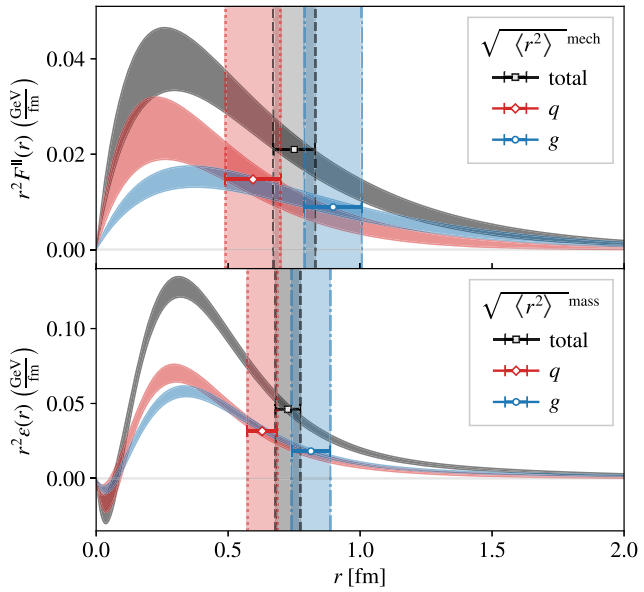

FIG. 3. The quark, gluon, and total contributions to the longitudinal force (upper) and energy (lower) densities in the Breit frame, computed on the lattice QCD ensemble of this Letter, are shown as functions of the radial distance from the center of the proton. The corresponding quark, gluon, and total mechanical and mass radii are marked as data points on the corresponding curves.

while the contributions of quarks and gluons to the proton's momentum, spin, and D term are approximately equal, the gluon contributions act to extend the radial size of the proton over that defined by the quark contributions as quantified through the mass and mechanical radii encoded in the t dependence of the GFFs. To improve upon these

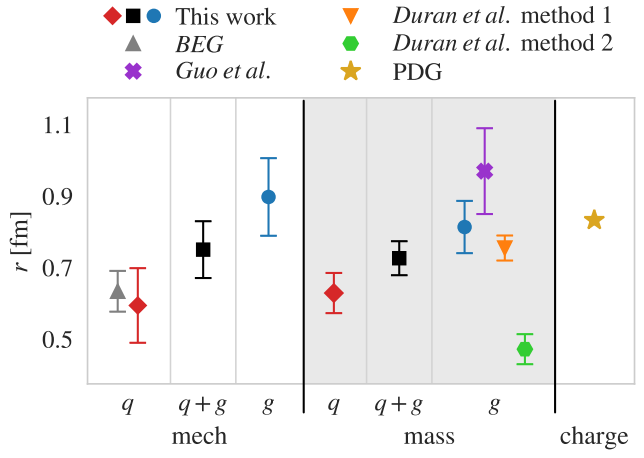

FIG. 4. Comparison of different proton radii. In addition to the results obtained on the lattice QCD ensemble of this Letter, the charge radius from Ref. [90] (PDG), the gluonic mass radii from Refs. [42] (Duran *et al.*) and [46] (Guo *et al.*), and the quark mechanical radii from Ref. [89] (BEG) are shown. While the latter includes only the light-quark contributions, they are compared directly, as the strange-quark contribution is found to be negligible for this quantity. The uncertainty of the charge radius is too small to be visible.

first results, it is crucial that this Letter be repeated using ensembles with different lattice volumes and lattice spacings in order for these systematic uncertainties to be fully accounted for. Moreover, it will be important to improve the renormalization procedure, e.g., by exploring the use of gauge-invariant renormalization schemes [91]. Nevertheless, these first-principles results permit first comparisons between theory and experiment for several aspects of these fundamental measures of proton structure.

The lattice QCD results for the $D_{u+d}(t)$ and $D_g(t)$ GFFs are consistent with the recent experimental results of Refs. [24,42], but $D_{u+d}(t)$ is constrained over a greater kinematic range. For $A_g(t)$, however, the comparison of first-principles theory with the experimental results of Ref. [42] provides important additional constraints that distinguish between different analyses of the experimental data. Moreover, the results for the separate up-, down-, and strange-quark GFFs presented here are the first constraints on these quantities from first-principles theory or from experiment. This Letter, thus, sets important benchmarks on these fundamental aspects of proton structure for future measurements at Thomas Jefferson National Accelerator Facility [92–94] and at a future Electron-Ion Collider [95].

The authors thank Will Detmold, Zein-Eddine Meziani, and Ross Young for useful feedback and suggestions. This work is supported in part by the U.S. Department of Energy, Office of Science, Office of Nuclear Physics, under Grant Contract No. DE-SC0011090 and by Early Career Award No. DE-SC0021006, and has benefited from the QGT Topical Collaboration DE-SC0023646. P. E. S. is supported in part by Simons Foundation Grant No. 994314 (Simons Collaboration on Confinement and QCD Strings) and by the U.S. Department of Energy SciDAC5 Award No. DE-SC0023116. D. A. P. is supported from the Office of Nuclear Physics, Department of Energy, under Contract No. DE-SC0004658. This manuscript has been authored by Fermi Research Alliance, LLC under Contract No. DE-AC02-07CH11359 with the U.S. Department of Energy, Office of Science, Office of High Energy Physics. This research used resources of the National Energy Research Scientific Computing Center (NERSC), a U.S. Department of Energy Office of Science User Facility operated under Contract No. DE-AC02-05CH11231, as well as resources of the Argonne Leadership Computing Facility, which is a DOE Office of Science User Facility supported under Contract No. DE-AC02-06CH11357, and the Extreme Science and Engineering Discovery Environment (XSEDE), which is supported by National Science Foundation Grant No. ACI-1548562. Computations were carried out in part on facilities of the USQCD Collaboration, which are funded by the Office of Science of the U.S. Department of Energy. The authors thank Robert Edwards, Rajan Gupta, Balint Joó, Kostas Orginos, and the NPLQCD Collaboration for generating the ensemble used in this study and Eloy Romero for assistance with software deployment. The Chroma [96],

QLua [97], QUDA [98–100], QDP-JIT [101], QPhiX [102], and Chromaform [103] software libraries were used in this work. Code for disconnected diagrams was adapted from LALIBE [104], including the hierarchical probing implementation by Andreas Stathopoulos [59]. Data analysis used NUMPY [105], SCIPY [106], PANDAS [107,108], LSQFIT [109], and GVAR [110]. Figures were produced using MATPLOTLIB [111].

[1] M. J. Neubelt, A. Sampino, J. Hudson, K. Tezgin, and P. Schweitzer, Energy momentum tensor and the D-term in the bag model, Phys. Rev. D **101**, 034013 (2020).
[2] M. V. Polyakov and H.-D. Son, Nucleon gravitational form factors from instantons: Forces between quark and gluon subsystems, J. High Energy Phys. 09 (2018) 156.
[3] K. Azizi and U. Özdem, Nucleon's energy–momentum tensor form factors in light-cone QCD, Eur. Phys. J. C **80**, 104 (2020).
[4] M. Fujita, Y. Hatta, S. Sugimoto, and T. Ueda, Nucleon D-term in holographic quantum chromodynamics, Prog. Theor. Exp. Phys. **2022**, 093B06 (2022).
[5] A. Amor-Quiroz, W. Focillon, C. Lorcé, and S. Rodini, Energy-momentum tensor in the scalar diquark model, Eur. Phys. J. C **83**, 1012 (2023).
[6] D. Chakrabarti, C. Mondal, A. Mukherjee, S. Nair, and X. Zhao, Gravitational form factors and mechanical properties of proton in a light-front quark-diquark model, Phys. Rev. D **102**, 113011 (2020).
[7] P. Choudhary, B. Gurjar, D. Chakrabarti, and A. Mukherjee, Gravitational form factors and mechanical properties of the proton: Connections between distributions in 2D and 3D, Phys. Rev. D **106**, 076004 (2022).
[8] C. Lorcé, P. Schweitzer, and K. Tezgin, 2D energy-momentum tensor distributions of nucleon in a large-Nc quark model from ultrarelativistic to nonrelativistic limit, Phys. Rev. D **106**, 014012 (2022).
[9] S. Owa, A. W. Thomas, and X. G. Wang, Effect of the pion field on the distributions of pressure and shear in the proton, Phys. Lett. B **829**, 137136 (2022).
[10] I. V. Anikin, Gravitational form factors within light-cone sum rules at leading order, Phys. Rev. D **99**, 094026 (2019).
[11] H.-Y. Won, J.-Y. Kim, and H.-C. Kim, Gravitational form factors of the baryon octet with flavor SU(3) symmetry breaking, Phys. Rev. D **106**, 114009 (2022).
[12] R. Fiore, L. Jenkovszky, and M. Oleksiienko, On matter and pressure distribution in nucleons, arXiv:2112.00605.
[13] K. A. Mamo and I. Zahed, Diffractive photoproduction of J/ψ and Υ using holographic QCD: Gravitational form factors and GPD of gluons in the proton, Phys. Rev. D **101**, 086003 (2020).
[14] K. A. Mamo and I. Zahed, J/ψ near threshold in holographic QCD: A and D gravitational form factors, Phys. Rev. D **106**, 086004 (2022).
[15] K. A. Mamo and I. Zahed, Nucleon mass radii and distribution: Holographic QCD, Lattice QCD and GlueX data, Phys. Rev. D **103**, 094010 (2021).
[16] G. F. de Téramond, H. G. Dosch, T. Liu, R. S. Sufian, S. J. Brodsky, and A. Deur (HLFHS Collaboration), Gluon matter distribution in the proton and pion from extended holographic light-front QCD, Phys. Rev. D **104**, 114005 (2021).
[17] C. Alexandrou *et al.*, Moments of nucleon generalized parton distributions from lattice QCD simulations at physical pion mass, Phys. Rev. D **101**, 034519 (2020).
[18] P. E. Shanahan and W. Detmold, Pressure distribution and shear forces inside the proton, Phys. Rev. Lett. **122**, 072003 (2019).
[19] P. E. Shanahan and W. Detmold, Gluon gravitational form factors of the nucleon and the pion from lattice QCD, Phys. Rev. D **99**, 014511 (2019).
[20] D. A. Pefkou, D. C. Hackett, and P. E. Shanahan, Gluon gravitational structure of hadrons of different spin, Phys. Rev. D **105**, 054509 (2022).
[21] G. S. Bali, S. Collins, M. Göckeler, R. Rödl, A. Schäfer, and A. Sternbeck, Nucleon generalized form factors from two-flavor lattice QCD, Phys. Rev. D **100**, 014507 (2019).
[22] H.-Y. Won, H.-C. Kim, and J.-Y. Kim, Mechanical structure of the nucleon and the baryon octet, J. High Energy Phys. 05 (2024) 173.
[23] Y. Guo, X. Ji, and F. Yuan, Proton's gluon GPDs at large skewness and gravitational form factors from near threshold heavy quarkonium photoproduction, Phys. Rev. D **109**, 014014 (2024).
[24] V. Burkert, L. Elouadrhiri, and F. Girod, The pressure distribution inside the proton, Nature (London) **557**, 396 (2018).
[25] C. Lorcé, H. Moutarde, and A. P. Trawiński, Revisiting the mechanical properties of the nucleon, Eur. Phys. J. C **79**, 89 (2019).
[26] M. Polyakov, Generalized parton distributions and strong forces inside nucleons and nuclei, Phys. Lett. B **555**, 57 (2003).
[27] M. V. Polyakov and P. Schweitzer, Forces inside hadrons: Pressure, surface tension, mechanical radius, and all that, Int. J. Mod. Phys. A **33**, 1830025 (2018).
[28] V. D. Burkert, L. Elouadrhiri, F. X. Girod, C. Lorcé, P. Schweitzer, and P. E. Shanahan, Colloquium: Gravitational form factors of the proton, Rev. Mod. Phys. **95**, 041002 (2023).
[29] N. K. Nielsen, The energy momentum tensor in a non-Abelian quark gluon theory, Nucl. Phys. **B120**, 212 (1977).
[30] F. J. Belinfante, Consequences of the postulate of a complete commuting set of observables in quantum electrodynamics, Phys. Rev. **128**, 2832 (1962).
[31] D. Müller, D. Robaschik, B. Geyer, F. M. Dittes, and J. Hořejši, Wave functions, evolution equations and evolution kernels from light ray operators of QCD, Fortschr. Phys. **42**, 101 (1994).
[32] X.-D. Ji, Gauge-invariant decomposition of nucleon spin, Phys. Rev. Lett. **78**, 610 (1997).
[33] A. V. Radyushkin, Scaling limit of deeply virtual Compton scattering, Phys. Lett. B **380**, 417 (1996).
[34] B. L. G. Bakker, E. Leader, and T. L. Trueman, A critique of the angular momentum sum rules and a new angular momentum sum rule, Phys. Rev. D **70**, 114001 (2004).
[35] I. Y. Kobzarev and L. B. Okun, Gravitational interaction of fermions, Zh. Eksp. Teor. Fiz. **43**, 1904 (1962).
[36] H. Pagels, Energy-momentum structure form factors of particles, Phys. Rev. **144**, 1250 (1966).

[37] M. V. Polyakov and C. Weiss, Skewed and double distributions in pion and nucleon, Phys. Rev. D **60**, 114017 (1999).

[38] Z. Fan, H.-W. Lin, and M. Zeilbeck, Nonperturbatively renormalized nucleon gluon momentum fraction in the continuum limit of Nf $= 2 + 1 + 1$ lattice QCD, Phys. Rev. D **107**, 034505 (2023).

[39] J. J. Ethier and E. R. Nocera, Parton distributions in nucleons and nuclei, Annu. Rev. Nucl. Part. Sci. **70**, 43 (2020).

[40] W. Detmold, R. G. Edwards, J. J. Dudek, M. Engelhardt, H.-W. Lin, S. Meinel, K. Orginos, and P. Shanahan (USQCD), Hadrons and nuclei, Eur. Phys. J. A **55**, 193 (2019).

[41] K.-F. Liu, Status on lattice calculations of the proton spin decomposition, AAPPS Bull. **32**, 8 (2022).

[42] B. Duran *et al.*, Determining the gluonic gravitational form factors of the proton, Nature (London) **615**, 813 (2023).

[43] P. Hagler *et al.* (LHPC Collaboration), Nucleon generalized parton distributions from full lattice QCD, Phys. Rev. D **77**, 094502 (2008).

[44] H.-W. Lin, Nucleon tomography and generalized parton distribution at physical pion mass from lattice QCD, Phys. Rev. Lett. **127**, 182001 (2021).

[45] C. Alexandrou *et al.*, Moments of the nucleon transverse quark spin densities using lattice QCD, Phys. Rev. D **107**, 054504 (2023).

[46] Y. Guo, X. Ji, Y. Liu, and J. Yang, Updated analysis of near-threshold heavy quarkonium production for probe of proton's gluonic gravitational form factors, Phys. Rev. D **108**, 034003 (2023).

[47] R. Edwards, R. Gupta, N. Joó, K. Orginos, D. Richards, F. Winter, and B. Yoon, U.s. $2 + 1$ flavor clover lattice generation program (unpublished).

[48] M. Lüscher and P. Weisz, On-shell improved lattice gauge theories, Commun. Math. Phys. **97**, 59 (1985); **98**, 433(E) (1985).

[49] B. Sheikholeslami and R. Wohlert, Improved continuum limit lattice action for QCD with Wilson fermions, Nucl. Phys. **B259**, 572 (1985).

[50] C. Morningstar and M. J. Peardon, Analytic smearing of SU(3) link variables in lattice QCD, Phys. Rev. D **69**, 054501 (2004).

[51] S. Park, R. Gupta, B. Yoon, S. Mondal, T. Bhattacharya, Y.-C. Jang, B. Joó, and F. Winter (Nucleon Matrix Elements (NME) Collaboration), Precision nucleon charges and form factors using $(2 + 1)$-flavor lattice QCD, Phys. Rev. D **105**, 054505 (2022).

[52] S. Borsanyi *et al.* (BMW Collaboration), High-precision scale setting in lattice QCD, J. High Energy Phys. 09 (2012) 010.

[53] D. C. Hackett, P. R. Oare, D. A. Pefkou, and P. E. Shanahan, Gravitational form factors of the pion from lattice QCD, Phys. Rev. D **108**, 114504 (2023).

[54] See Supplemental Material at http://link.aps.org/supplemental/10.1103/PhysRevLett.132.251904 for additional analysis details and discussion.

[55] M. Lüscher, Properties and uses of the Wilson flow in lattice QCD, J. High Energy Phys. 08 (2010) 071; 03 (2014) 92.

[56] R. Narayanan and H. Neuberger, Infinite N phase transitions in continuum Wilson loop operators, J. High Energy Phys. 03 (2006) 064.

[57] R. Lohmayer and H. Neuberger, Continuous smearing of Wilson Loops, Proc. Sci., Lattice2011 (**2012**) 249 [arXiv:1110.3522].

[58] M. Hutchinson, A stochastic estimator of the trace of the influence matrix for Laplacian smoothing splines, Commun. Stat. Simul. Comput. **19**, 433 (1990).

[59] A. Stathopoulos, J. Laeuchli, and K. Orginos, Hierarchical probing for estimating the trace of the matrix inverse on toroidal lattices, SIAM J. Sci. Comput. **35**, S299 (2013).

[60] A. S. Gambhir, Disconnected diagrams in lattice QCD, Ph.D. thesis, William-Mary Coll., 2017.

[61] S. Capitani, M. Della Morte, G. von Hippel, B. Jäger, A. Juttner, B. Knippschild, H. B. Meyer, and H. Wittig, The nucleon axial charge from lattice QCD with controlled errors, Phys. Rev. D **86**, 074502 (2012).

[62] L. Maiani, G. Martinelli, M. L. Paciello, and B. Taglienti, Scalar densities and baryon mass differences in lattice QCD with Wilson fermions, Nucl. Phys. **B293**, 420 (1987).

[63] S. J. Dong, K. F. Liu, and A. G. Williams, Lattice calculation of the strangeness magnetic moment of the nucleon, Phys. Rev. D **58**, 074504 (1998).

[64] D. Djukanovic, T. Harris, G. von Hippel, P. M. Junnarkar, H. B. Meyer, D. Mohler, K. Ottnad, T. Schulz, J. Wilhelm, and H. Wittig, Isovector electromagnetic form factors of the nucleon from lattice QCD and the proton radius puzzle, Phys. Rev. D **103**, 094522 (2021).

[65] H. Akaike, *Information Theory and an Extension of the Maximum Likelihood Principle* (Springer Science+ Business Media, New York, 1998).

[66] W. I. Jay and E. T. Neil, Bayesian model averaging for analysis of lattice field theory results, Phys. Rev. D **103**, 114502 (2021).

[67] E. Rinaldi, S. Syritsyn, M. L. Wagman, M. I. Buchoff, C. Schroeder, and J. Wasem, Neutron-antineutron oscillations from lattice QCD, Phys. Rev. Lett. **122**, 162001 (2019).

[68] S. R. Beane, E. Chang, W. Detmold, K. Orginos, A. Parreño, M. J. Savage, and B. C. Tiburzi (NPLQCD Collaboration), *Ab initio* calculation of the np $\rightarrow$ dγ radiative capture process, Phys. Rev. Lett. **115**, 132001 (2015).

[69] D. Steinberg, kmeans1d, https://github.com/dstein64/kmeans1d (2019).

[70] R. J. Hill and G. Paz, Model independent extraction of the proton charge radius from electron scattering, Phys. Rev. D **82**, 113005 (2010).

[71] G. Wang, Y.-B. Yang, J. Liang, T. Draper, and K.-F. Liu (χQCD), Proton momentum and angular momentum decompositions with overlap fermions, Phys. Rev. D **106**, 014512 (2022).

[72] C. Alexandrou, S. Bacchio, M. Constantinou, J. Finkenrath, K. Hadjiyiannakou, K. Jansen, G. Koutsou, H. Panagopoulos, and G. Spanoudes, Complete flavor decomposition of the spin and momentum fraction of the proton using lattice QCD simulations at physical pion mass, Phys. Rev. D **101**, 094513 (2020).

[73] T.-J. Hou *et al.*, New CTEQ global analysis of quantum chromodynamics with high-precision data from the LHC, Phys. Rev. D **103**, 014013 (2021).

[74] J. Gegelia and M. V. Polyakov, A bound on the nucleon Druck-term from chiral EFT in curved space-time and

mechanical stability conditions, Phys. Lett. B **820**, 136572 (2021).
[75] K. Goeke, J. Grabis, J. Ossmann, M. V. Polyakov, P. Schweitzer, A. Silva, and D. Urbano, Nucleon form-factors of the energy momentum tensor in the chiral quark-soliton model, Phys. Rev. D **75**, 094021 (2007).
[76] P. Schweitzer, S. Boffi, and M. Radici, Polynomiality of unpolarized off forward distribution functions and the D term in the chiral quark soliton model, Phys. Rev. D **66**, 114004 (2002).
[77] J. Ossmann, M. V. Polyakov, P. Schweitzer, D. Urbano, and K. Goeke, The generalized parton distribution function $(E^u + E^d)(\mathrm{x}, \mathrm{xi}, \mathrm{t})$ of the nucleon in the chiral quark soliton model, Phys. Rev. D **71**, 034011 (2005).
[78] K. Goeke, J. Grabis, J. Ossmann, P. Schweitzer, A. Silva, and D. Urbano, The pion mass dependence of the nucleon form-factors of the energy momentum tensor in the chiral quark-soliton model, Phys. Rev. C **75**, 055207 (2007).
[79] M. Wakamatsu, On the D-term of the nucleon generalized parton distributions, Phys. Lett. B **648**, 181 (2007).
[80] C. Cebulla, K. Goeke, J. Ossmann, and P. Schweitzer, The nucleon form-factors of the energy momentum tensor in the Skyrme model, Nucl. Phys. **A794**, 87 (2007).
[81] J.-H. Jung, U. Yakhshiev, and H.-C. Kim, Energy–momentum tensor form factors of the nucleon within a π-ρ-ω soliton model, J. Phys. G **41**, 055107 (2014).
[82] P. Chatagnon *et al.* (CLAS Collaboration), First measurement of timelike Compton scattering, Phys. Rev. Lett. **127**, 262501 (2021).
[83] Y. Guo, X. Ji, and Y. Liu, QCD analysis of near-threshold photon-proton production of heavy quarkonium, Phys. Rev. D **103**, 096010 (2021).
[84] S. Adhikari *et al.* (GlueX Collaboration), Measurement of the J/ψ photoproduction cross section over the full near-threshold kinematic region, Phys. Rev. C **108**, 025201 (2023).
[85] X. Ji and Y. Liu, Momentum-current gravitational multipoles of hadrons, Phys. Rev. D **106**, 034028 (2022).
[86] R. L. Jaffe, Ambiguities in the definition of local spatial densities in light hadrons, Phys. Rev. D **103**, 016017 (2021).
[87] J. Y. Panteleeva, E. Epelbaum, J. Gegelia, and U. G. Meißner, Definition of gravitational local spatial densities for spin-0 and spin-1/2 systems, Eur. Phys. J. C **83**, 617 (2023).
[88] A. Freese and G. A. Miller, Unified formalism for electromagnetic and gravitational probes: Densities, Phys. Rev. D **105**, 014003 (2022).
[89] V. D. Burkert, L. Elouadrhiri, and F. X. Girod, The mechanical radius of the proton, arXiv:2310.11568.
[90] R. L. Workman *et al.* (Particle Data Group), Review of particle physics, Prog. Theor. Exp. Phys. **2022**, 083C01 (2022).
[91] M. Costa, I. Karpasitis, T. Pafitis, G. Panagopoulos, H. Panagopoulos, A. Skouroupathis, and G. Spanoudes, Gauge-invariant renormalization scheme in QCD: Application to fermion bilinears and the energy-momentum tensor, Phys. Rev. D **103**, 094509 (2021).
[92] J. Arrington *et al.* (Jefferson Lab SoLID Collaboration), The solenoidal large intensity device (SoLID) for JLab 12 GeV, J. Phys. G **50**, 110501 (2023).
[93] V. D. Burkert, Jefferson lab at 12 GeV: The science program, Annu. Rev. Nucl. Part. Sci. **68**, 405 (2018).
[94] J. Arrington *et al.*, Physics with CEBAF at 12 GeV and future opportunities, Prog. Part. Nucl. Phys. **127**, 103985 (2022).
[95] R. Abdul Khalek *et al.*, Science requirements and detector concepts for the electron-ion collider: EIC Yellow Report, Nucl. Phys. **A1026**, 122447 (2022).
[96] R. G. Edwards and B. Joó (SciDAC, LHPC, and UKQCD Collaborations), The Chroma software system for lattice QCD, Nucl. Phys. B, Proc. Suppl. **140**, 832 (2005).
[97] A. Pochinsky, Qlua, https://usqcd.lns.mit.edu/qlua.
[98] M. Clark, R. Babich, K. Barros, R. Brower, and C. Rebbi, Solving lattice QCD systems of equations using mixed precision solvers on GPUs, Comput. Phys. Commun. **181**, 1517 (2010).
[99] R. Babich, M. Clark, B. Joó, G. Shi, R. Brower, and S. Gottlieb, Scaling lattice QCD beyond 100 GPUs, in *Proceedings of the SC11 International Conference for High Performance Computing, Networking, Storage and Analysis* (2011), arXiv:1109.2935.
[100] M. A. Clark, B. Joó, A. Strelchenko, M. Cheng, A. Gambhir, and R. Brower, Accelerating lattice QCD multigrid on GPUs using fine-grained parallelization, arXiv:1612.07873.
[101] B. Joó, D. D. Kalamkar, T. Kurth, K. Vaidyanathan, and A. Walden, Optimizing wilson-dirac operator and linear solvers for intel®knl, in *High Performance Computing*, edited by M. Taufer, B. Mohr, and J. M. Kunkel (Springer International Publishing, Cham, 2016), pp. 415–427.
[102] B. Joó, D. D. Kalamkar, T. Kurth, K. Vaidyanathan, and A. Walden, Optimizing Wilson-Dirac operator and linear solvers for intel® knl, in *High Performance Computing*, edited by M. Taufer, B. Mohr, and J. M. Kunkel (Springer International Publishing, Cham, 2016), pp. 415–427.
[103] E. Romero and C. Kallidonis, chromaform, https://github.com/eromero-vlc/chromaform.
[104] A. Gambhir, D. Brantley, J. Chang, B. Hörz, H. Monge-Camacho, P. Vranas, and A. Walker-Loud, lalibe, https://github.com/callat-qcd/lalibe (2018).
[105] C. R. Harris *et al.*, Array programming with NUMPY, Nature (London) **585**, 357 (2020).
[106] P. Virtanen *et al.* (SCIPY1.0 Contributors), SCIPY1.0: Fundamental algorithms for scientific computing in PYTHON, Nat. Methods **17**, 261 (2020).
[107] J. Reback *et al.*, pandas-dev/pandas: PANDAS1.0.3 (2020), 10.5281/zenodo.3715232.
[108] Wes McKinney, Data structures for statistical computing in PYTHON, in *Proceedings of the 9th PYTHON in Science Conference*, edited by Stéfan van der Walt and Jarrod Millman (2010), pp. 56–61.
[109] G. P. Lepage, LSQFITv.11.7 (2020), https://github.com/gplepage/lsqfit, 10.5281/zenodo.4037174.
[110] G. P. Lepage, GVARv.11.9.1 (2020), https://github.com/gplepage/gvar, 10.5281/zenodo.4290884.
[111] J. D. Hunter, MATPLOTLIB: A 2d graphics environment, Comput. Sci. Eng. **9**, 90 (2007).